Geophysical Research Letters

RESEARCH LETTER
10.1029/2022GL100898

Key Points:

- Continuous dipole moment models for the past 3.7–4.2 billion years are presented
- Our model reproduces salient features of the paleomagnetic dipole field
- Paleomagnetosphere estimates suggest Precambrian atmospheric shielding was much weaker than present day

Supporting Information:

Supporting Information may be found in the online version of this article.

Correspondence to:

R. K. Bono,
rbono@fsu.edu

Citation:

Bono, R. K., Paterson, G. A., & Biggin, A. J. (2022). MCADAM: A continuous paleomagnetic dipole moment model for at least 3.7 billion years. *Geophysical Research Letters*, *49*, e2022GL100898. https://doi.org/10.1029/2022GL100898

Received 30 AUG 2022
Accepted 29 OCT 2022

MCADAM: A Continuous Paleomagnetic Dipole Moment Model for at Least 3.7 Billion Years

Richard K. Bono[1], Greig A. Paterson[2], and Andrew J. Biggin[2]

[1]Department of Earth, Ocean and Atmospheric Science, Florida State University, Tallahassee, FL, USA, [2]Department of Earth, Ocean and Ecological Sciences, University of Liverpool, Liverpool, UK

Abstract Understanding the evolution of Earth's magnetic field can provide insights into core processes and can constrain plate tectonics and atmospheric shielding. The absolute paleointensity database PINT provides a curated repository of site mean (i.e., cooling unit), estimates of the strength of the magnetic field. We present a minor update to the PINT database to version 8.1.1 by adding 295 records from 34 studies. The PINT database is used to define a continuous model of the dipole field, using an approach combining non-parametric and Monte Carlo (MC) resampling termed Monte Carlo Axial Dipole Average Model (MCADAM). Three dipole field strength models spanning 50 ka to 3.7–4.2 Ga (MCADAM.1a-c) are presented, reflecting three tiers of increasingly more stringent data selection. The MCADAM models allow for the estimation of the magnetic standoff distance, constraining the shielding of Earth's atmosphere against solar wind erosion provided by the geodynamo.

Plain Language Summary The geomagnetic field is a long-lived feature that provides critical shielding of Earth's atmosphere from solar wind erosion. Understanding changes in field strength can provide insight into the evolution of Earth's core. Here we use an updated database of paleointensity estimates to develop new continuous models of the strength of Earth's magnetic field. These models include plausible uncertainties, and capture variations in field strength spanning 50 thousand to over 3.7 billion years ago. Using our models, we suggest that the atmospheric shielding provided by the field was about 60% the present-day shielding for most of the Precambrian.

1. Introduction

The evolution of Earth's deep interior since core formation (Nimmo, 2015) >4 billion years ago (Ga) remains a topic of considerable study. Obtaining information of the deep interior is generally restricted to present-day observations. Alternatively, insights on processes occurring before the modern era require sampling geologic materials that formed at, or were transported to, Earth's surface. However, the geomagnetic field is generated in the liquid fraction of Earth's core through the geodynamo, and changes in the morphology, strength and variability in the geodynamo may reflect the evolution of core processes and the pattern of heat flux across the core-mantle boundary. The geomagnetic field is also a critical component for Earth's habitability (Rodríguez-Mozos & Moya, 2017) due to the protective envelope provided by the magnetosphere against atmospheric erosion by charged solar particles. It is speculated that changes in the paleomagnetosphere may have contributed to substantial changes in the evolution of life (e.g., Meert et al., 2016).

Paleomagnetic studies offer the potential to help close this gap: when rocks bearing magnetic carriers form, the geomagnetic field imparts a remanent magnetization that under ideal circumstances can be robustly preserved for billions of years. The strength of the geodynamo can be described by the magnitude of the dipole moment, the first-degree spherical harmonic component of the field, which should reflect ~90% of the surface field signal. A fundamental question regarding Earth's dynamo is how the dipole moment has changed over long timescales (≫millions of years). Paleointensities measured from the same geologic time (e.g., from the same cooling-unit, referred to as a "site") can be related to paleointensities from other locations by transforming the paleointensity (B) into a virtual (axial) dipole moment (V(A)DM) using the following equation (Smith, 1967):

$$VDM = \frac{4\pi {R_E}^3}{2\mu_0} B\left(1 + 3\cos^2 I\right)^{0.5}, \quad (1)$$

where R_E is Earth's radius, μ_0 is vacuum permeability, and I is the inclination of the site derived from paleomagnetic directional measurements (there is an equivalent transformation to VADM using site paleolatitude; Merrill et al., 1996). Virtual dipole moment transformations assert that the mean paleointensity measured at the site level can be entirely described by the dipole field, this simplification allows for comparisons of globally distributed observations of field strength.

Characterizing the time-varying paleomagnetic field can be approached using several different methods. On geologically recent timescales (<100 thousand years, Kyr), spherical harmonic models describe the morphology and strength of the field (e.g., Panovska et al., 2018). For the past 2 Myr, a continuous axial dipole moment model (Ziegler et al., 2011) can be constructed using relative paleointensity data from stacked sedimentary records combined with absolute paleointensity estimates, generally from volcanic sources. For longer timescales (≫2 million years), dipole moment descriptions are substantially less well resolved. Tauxe and Staudigel (2004) report a mean value for the 0–300 Ma interval, whereas Ingham et al. (2014) and Kulakov et al. (2019) applied a more complex reversible-jump Markov Chain Monte Carlo (MC) approach to define Mesozoic trends. Other approaches, applied to the Precambrian field, include binned data (e.g., Biggin et al., 2015), a low-degree polynomial fit (e.g., Bono et al., 2019), or sliding window average (e.g., Tarduno et al., 2020). These meta-analyses have proven important in providing observational constraints on dynamo and core evolution models (e.g., Biggin et al., 2015; Bono et al., 2019; Driscoll, 2016) and time-averaged and time-varying field estimates (e.g., Selkin & Tauxe, 2000; Ziegler et al., 2011).

In this study, we provide a minor version update to the PINT database (http://www.pintdb.org/; Biggin et al., 2009; Bono et al., 2022) that we use as the basis for a dipole moment evolution model (Section 2). In Section 3, we introduce a modeling framework, MCADAM (Monte Carlo Axial Dipole Average Model), that uses a combination of non-parametric site resampling, MC simulations, and time-adaptive locally weighted smoothing to produce a posterior distribution of field strength estimates from which a median dipole strength and associated predictive interval can be determined. Using the MCADAM framework and three filtered data sets from the PINT database that apply increasingly more stringent selection criteria, we present a suite of dipole moment evolution models that yield continuous predictions of the time-average (paleomagnetic) dipole moment extending back to the oldest paleomagnetic records from >4 Ga, and compare these models with other time-average descriptions of field strength in deep time (Section 4) and the associated impact on the paleomagnetosphere (Section 5).

2. Updates to PINT v8.1.1

The PINT database, a curated repository of absolute paleointensity records derived from volcanic sources and reported at the site mean level with associated meta-data, underwent a significant update to version 8.0.0, and we refer readers to Bono et al. (2022) who describe the current structure of the database and broadly summarizes the distribution and quality of the paleointensity data set. The most salient changes in PINT v8.0.0 with respect to prior versions of the PINT database (Biggin et al., 2015) are the inclusion of new paleointensity data published through the end of 2019, the removal of demonstrably biased paleointensity records (so-called "auto-zeros"), and the integration of Q_{PI} assessments for over 90% of the database. Q_{PI} (Quality of Paleointensity; Biggin & Paterson, 2014) is a qualitative framework to describe the reliability of a site mean paleointensity record, and we again refer readers to Bono et al. (2022) for a complete description of Q_{PI} implementation in PINT v8.0.0.

In this study, we include a minor version update of PINT to v8.1.1 (Figure 1) that includes paleointensity records published in 2020 through August 2022. Included studies are not exhaustive of entire paleointensity data set published during this interval, however, it represents a good-faith effort to identify as many relevant studies as possible. In total, 295 new sites from 34 studies have been added to the PINT v8.1.1 database, increasing the total number of site mean records (N_{Sites}) to 4,648. These data include contributions constraining the field during the Cambrian/Ediacaran (e.g., Thallner, Biggin, & Halls, 2021; Thallner, Biggin, McCausland, & Fu, 2021; Thallner et al., 2022; Zhou et al., 2022) and Neoproterozoic (e.g., Lloyd, Biggin, et al., 2021), which remain under-sampled relative to other geologic intervals.

Q_{PI} criteria allow for a semi-quantitative, objective definition of requirements to filter data from the PINT database, with the goal of improving the robustness of meta-analyses (Biggin & Paterson, 2014; Bono et al., 2022). Field strength estimates are inherently challenging to extract from the rock record. Paleointensity specimens may be compromised by the presence of non-ideal magnetic recorders (e.g., multidomain grains) and/or laboratory

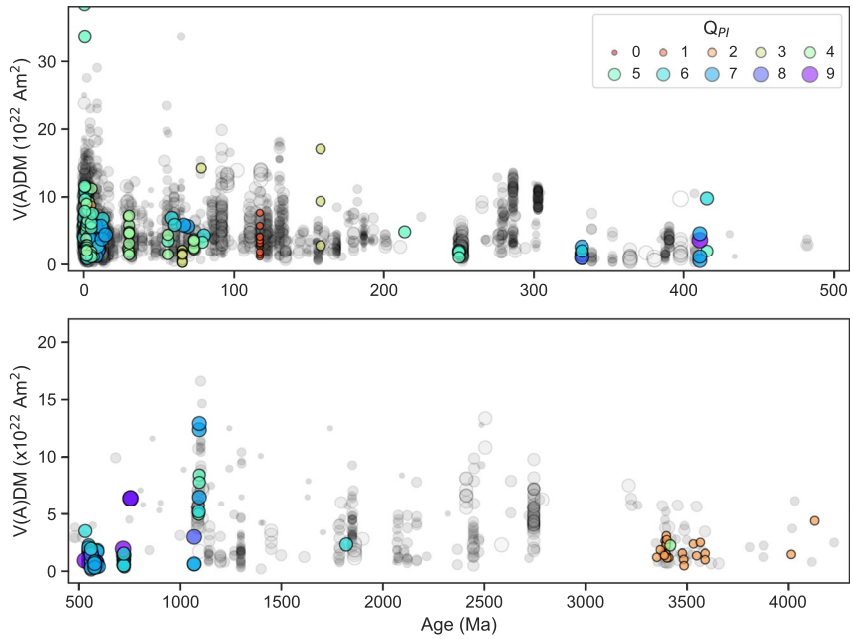

Figure 1. PINT v8.1.1 absolute paleointensity database. Colored circles show site mean records added since v8.0.0 (Bono et al., 2022); gray circles are data in v8.0.0. Symbol size and color shows Q_{PI} score. Top: Phanerozoic; bottom: Precambrian.

alteration. The potential for remanences to be reset by thermal or chemical over-printing after emplacement must also be excluded before accepting a measured paleointensity as valid and meaningfully linked to the emplacement age. Since the data may reflect some non-ideal paleointensity biases, some fraction of the site mean data should be excluded from analyses in order to improve the robustness of any resulting conclusions drawn from using the PINT database. However, paleointensity data are sparse and imperfect individual records may still yield meaningful inferences in aggregate. Thus it is crucial to define selection criteria that balance data quality with data availability, specifically for the development of time-averaged and time-evolution field descriptions on million-to-billion-year timescales. Meta-analyses considering other topics will, of course, result in different optimal selection criteria choice.

Three different selection criteria are employed for model development (previously presented in Bono et al. (2022)). In addition to the following selection criteria, sites explicitly described as having a transitional polarity were excluded from all data sets. The first two filters are (a) all data (N_{Sites}: 4,239) and (b) $Q_{PI} \geq 3$ (N_{Sites}: 2,327). The third filter (c), introduced by Kulakov et al. (2019), prioritizes records passing specific Q_{PI} criteria (N_{Sites}: 1,009). We require evidence that the site age is well constrained and the primary remanence is associated with the age estimate (QAGE) and there were experimental controls to limit the influence of laboratory alteration and non-ideal (i.e., multidomain) magnetic carriers. We note that Smirnov et al. (2016) and Bono et al. (2019) previously identified paleointensity data which potentially under (over) estimate field strength by fitting the shallow (steep) components of two-slope or concave Arai diagrams. Since this level of analysis was not applied to all records within PINT v8.1.1, we have not excluded the identified sites a priori, however, we distinguish sites that may be biased in Figure 2b and all but two sites are independently excluded using our "strict" prioritized Q_{PI} selection criteria.

3. Time-Varying Paleofield Models With Uncertainties

Here, we consider whether a continuous time-varying dipole moment model can be realized for the entire paleointensity record. Ideally, this model should take several factors into consideration; we chose to focus on the following requirements:

1. Data selection should balance quality with availability of data.
2. Not be overly sensitive to any given data point due to the sparse and non-uniform distribution of paleointensity site mean data.

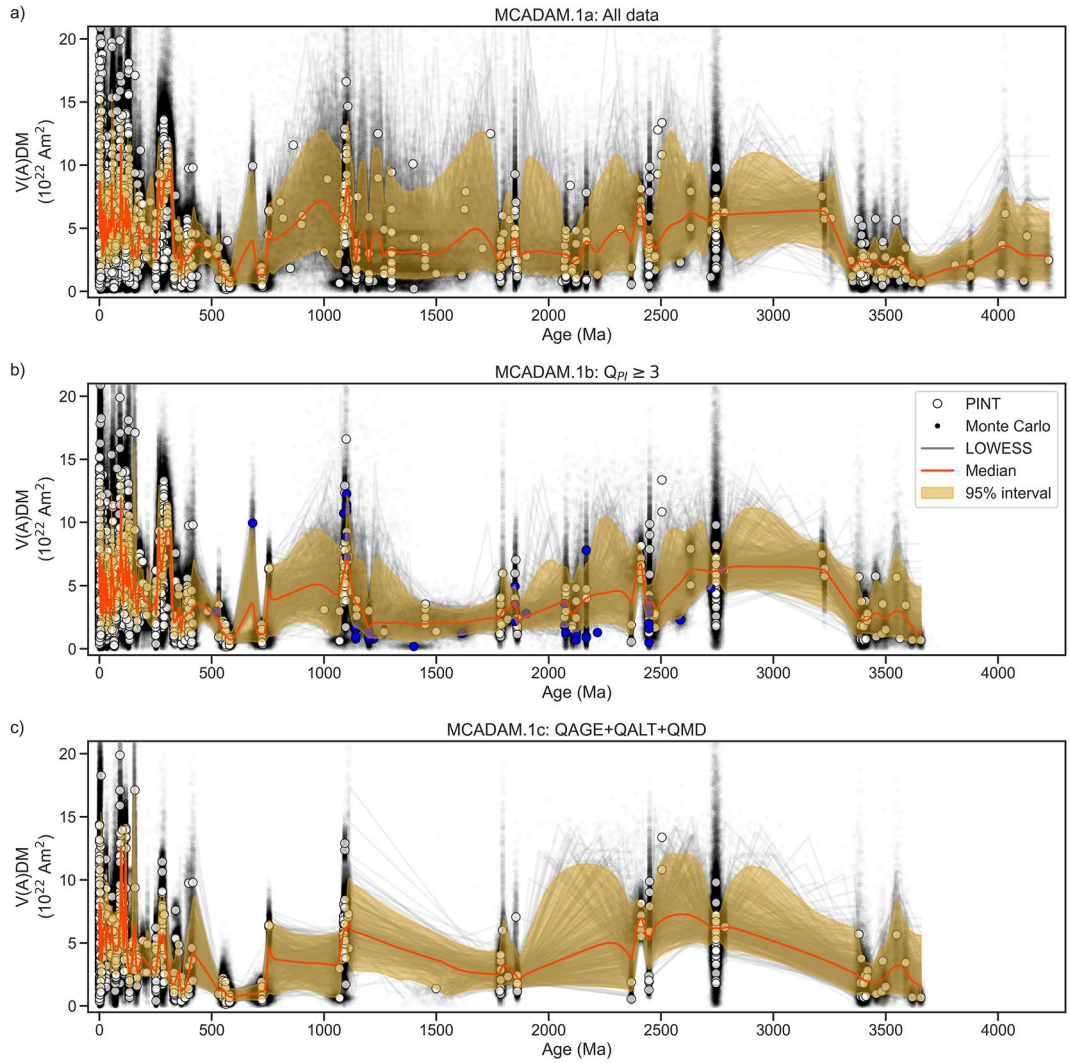

Figure 2. Monte Carlo Axial Dipole Average Model (MCADAM) time-varying model of dipole strength for the past 3.7 to 4.2 billion years from PINT v8.1.1 data. White circles: selected site mean virtual (axial) dipole moments (V(A)DMs); black points, Monte Carlo realizations; gray lines, individual interpolated realizations; orange line, median dipole moment with shaded 95% interval. (a) MCADAM.1a, all non-transitional polarity data in PINT v8.1.1; (b) MCADAM.1b, $Q_{\rm PI} \geq 3$, blue circles mark sites that may be biased as identified by Smirnov et al. (2016) or Bono et al. (2019); and (c) MCADAM.1c, prioritized $Q_{\rm PI}$.

3. Reflect the uncertainty of individual site mean estimates in both age and field strength.
4. Seek to average secular variation, taking into account the increasing sparsity of data going further back into geologic time.

To meet these requirements, we employ a combination of techniques, which we refer to as a MCADAM. The modeling framework was tested using a synthetic data set with a known "true" dipole moment and a temporal distribution derived from PINT v8.1.1 (Text S1 and Figure S1 in Supporting Information S1). The MCADAM time-varying model is constructed as follows:

1. Randomly resample the selected sites with replacement (bootstrap resampling, following Efron and Tibshirani (1993)). A non-parametric resampling approach is preferred since the temporal distribution of paleointensity records is highly non-uniform.
2. For each resampled site mean, we use MC resampling to generate a new dipole moment and age constrained by the site mean and variance. Each dipole moment realization is calculated from a random realization of inclination (drawn from a Fisher distribution with k precision parameter from the PINT record) and a site

mean field intensity (B) drawn from a normal distribution with a mean defined from the record. The variance for field strength, σ_B^2, is determined from the unbiased estimate of standard deviation (Holtzman, 1950). In cases where site mean inclination is unavailable, the MC realization is drawn from a distribution mimicking the latitudinal distribution of surface area on a sphere. In cases where paleointensity uncertainty is unavailable, σ_B is set to 60% of B (estimated from the 90th percentile of dBn(%) from the entire PINT database). Similarly, if there is no uncertainty in site mean age, a standard deviation of 10% the site mean age is assigned (arbitrarily chosen based on the upper uncertainty bound for QAGE).

3. A weighted average is found for each sample using the weighting kernel defined below, based on a LOWESS averaging method (Cleveland (1979); also described as a Savitzky and Golay (1964) filter). For each point in the resampled record, define a weighting kernel:
   - Kernel shape is defined using a tricube function where weights range from 0 to 1 centered on sample age with a prescribed bandwidth outside of which the weight is 0.
   - Bandwidth is defined as the minimum age interval that both samples at least five sites and the maximum of either 250 Kyr or 2% of the age of the site (e.g., at least 74 Myr at 3.7 Ga), up to a maximum of 500 Myr. If there are fewer than five sites within a 500 Myr interval, that point in the realization is dropped.
4. To ease compilation, since each realization will return different number and distribution of time steps, a linear interpolated curve with uniform, high-resolution time steps (here, 50 Kyr) is determined from the weighted average for each realization.
5. Steps 1–4 are repeated a large number of times (e.g., 10^4).
6. Average statistics (mean, standard deviation, median, mode, 75% and 95% intervals) for each step in the set of interpolated curves are determined.

4. Comparing MCADAM to Other Compilations

Applying the MCADAM approach with the PINT v8.1.1 data set restricted by the three selection filters previously discussed (Section 2), the resulting time-varying models (MCADAM.1a-c) are presented in Figure 2 and available for download in the EarthRef Data Archive (http://www.earthref.org/ERDA/2537/). Our preferred model is MCADAM.1b, which uses a moderately restrictive data selection requiring that paleointensity site records meet at least three of the Q_{PI} criteria. In general, these models reproduce several characteristic features previously observed in the paleofield (Figure 3 and Figures S2–S3 in Supporting Information S1), such as rise in field strength from the Matuyama to Brunhes chrons, intervals of high field strength during the Cretaceous Normal Superchron preceded by a weaker field (cf. Kulakov et al., 2019), and a high field during the Kiaman Superchron (e.g., Cottrell et al., 2008) preceded by sustained weak field during the Devonian (Hawkins et al., 2019). We note that the low field predictions prior to the CNS of Kulakov et al. (2019) are less pronounced and persist for a shorter interval in MCADAM. This is likely due to the incorporation of age uncertainty, the inherent smoothing of the LOWESS approach, and the inclusion of new data (e.g., Di Chiara et al., 2021) in the MCADAM model. For the 50 Kyr to 2 Ma interval, there is good agreement between our model and that of PADM2M (Ziegler et al., 2011). There is a small, apparently systematic difference between MCADAM and PADM2M, which lessens as more stringent data selection criteria are applied to MCADAM (cf. Figure 2a, Figures S2a and S3a in Supporting Information S1). We also note that PADM2M includes transitional data from absolute paleointensity data (i.e., records from PINT, as of 2011, excluded by MCADAM) and relative paleointensity records (i.e., sediment stacks recording excursions and the Brunhes-Matuyama reversal). The inclusion of transitional data in PADM2M precludes a direct quantitative comparison, since MCADAM is tuned to predict the time-averaged field that excludes transitional intervals. Given the denser temporal sampling during the Phanerozoic, more variation in the field can be resolved with a smaller confidence interval for the resulting model relative to the Precambrian.

The Paleozoic through the Precambrian poses the greatest challenge for characterizing the time-varying field due to large gaps in the PINT database. In our model, we use a linear interpolation between sampling, however given that intervals spanning ∼100 Myr may not sample the field at all, it is almost certain there are field variations that are not captured in our model. Given the combination of non-parametric resampling for site selection, the MC resampler, and locally weighted regression, therefore, the MCADAM should represent an overly smoothed description of the time varying field, particularly where the data are sparse. Despite our best efforts, in intervals when data is particularly sparse the model may be susceptible to bias from anomalous data. For example, in Figure 2, the difference between MCADAM.1b and MCADAM.1c at ∼680 Ma due to the contribution of a potentially biased record; the authors of the study reporting the anomalous site mean paleointensity, Salminen

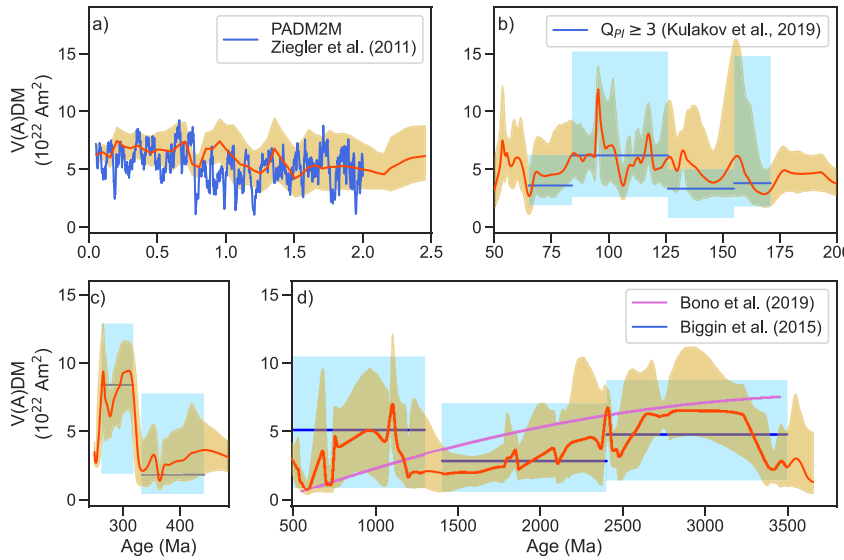

Figure 3. MCADAM.1b time-varying model of paleofield strength for the past 3.7 billion years from PINT v8.1.1 data meeting $Q_{PI} \geq 3$ criteria. In all panels, the orange line represents the median time-varying model from MCADAM.1b with shaded 95% interval. (a) Quaternary; blue line shows PADM2M model (Ziegler et al., 2011); (b) Mesozoic; blue line and field shows median and 95% interval estimates of (Kulakov et al., 2019); (c) Paleozoic excerpt; blue lines and fields show median and 95% confidence interval determined from PINT v8.1.1 for the Kiaman Superchron (318–262 Ma; e.g., Opdyke & Channell, 1996) and Mid-Paleozoic Dipole Low (442–332 Ma; Hawkins et al., 2021); and (d) Precambrian; purple line shows polynomial fit of Bono et al. (2019), blue lines show bin medians with shaded 95% confidence intervals of Biggin et al. (2015).

et al. (2006), explicitly acknowledge the potential for high-field bias in their data. We note that the oldest field records of the Archean are dominated by the Thellier-Coe zircon experiments of Tarduno et al. (2015); Tarduno et al. (2020), which due to their lack of orientation, represent a source of uncertainty in our model during the Eoarchean/Hadean. The fall and rise in field strength during the Mid- to Late-Proterozoic (as suggested by Biggin et al. (2015)) is supported by our model, as well as the drop in field strength at the end of the Proterozoic reported in Bono et al. (2019).

There are some general differences in the analyses of Biggin et al. (2015), Bono et al. (2019), and our study that can explain the apparent disagreement in estimated field trends. First, there are differences in the data sets used between both analyses, as summarized by Bono et al. (2019). Second, Biggin et al. (2015) divided the data sets into Early, Mid, and Late Proterozoic bins and summarized the statistical properties each bin. Bono et al. (2019) focused a priori on estimates from slow-cooling intrusives (or select sites demonstrating time-averaged statistics) resulting in a substantially reduced data set compared to either this study or Biggin et al. (2015), and from this restricted data set fit a second-degree polynomial trend. In this study, we forgo both dividing the data into prescribed bins or focusing a priori on intrinsically time-averaged records. Our study uses a broader data set, supplemented by new data published since the prior studies, that results in more variation in the interpreted dipole field strength relative to prior work.

5. Implications for the Paleomagnetosphere

The geodynamo and the associated magnetic field extending into space provides shielding of Earth's atmosphere and surface water from erosion due to solar wind (Tarduno et al., 2014). In addition to increasing erosion of the atmosphere, reductions in magnetic shielding can drive breakdown of atmospheric ozone, which limits penetration of UVB radiation (Glassmeier & Vogt, 2010). Currently, modeling the paleomagnetosphere in detail requires fully coupled dynamo and solar activity simulations beyond the scope of what is available. However, a first-order approximation can be estimated using a series of reasonable simplifications, chiefly that the field is axial dipole-dominated (Biggin et al., 2020) and that magnetic shielding can be approximated by the magnetic standoff distance, or magnetopause, where solar wind pressure is balanced by the repelling force of a dipole field

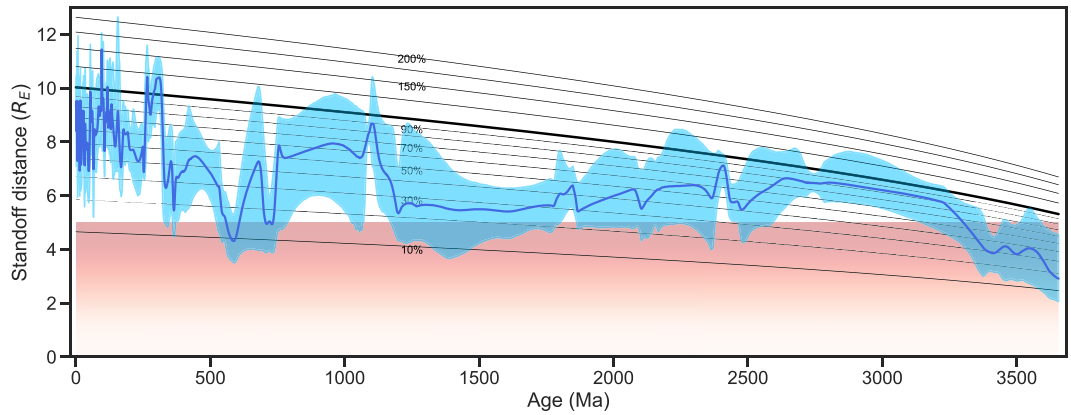

Figure 4. Magnetopause standoff distance estimate using Equation 2 and the MCADAM.1b modeled dipole moment curve with PINT v8.1.1 data meeting $Q_{PI} \geq 3$ criteria. Blue curve is the estimated magnetopause standoff distance using the predicted median dipole moment and blue field is the 95% predicted interval. Contour lines show standoff distance relative to the present day dipole field. Red gradient shows standoff distance associated with the Halloween 2003 solar storm (Rosenqvist et al., 2005).

(Siscoe & Sibeck, 1980). The present-day magnetopause is ~10 R_E (Earth radii) and will fluctuate on annual timescales as the magnetic pole moves about the spin axis (Shue et al., 1997).

Following the approach of Tarduno et al. (2010), the magnetic standoff distance, $R_s(t)$ for a given time t, can be estimated (Siscoe & Chen, 1975) by

$$R_s(t) = \left[\frac{\mu_0^2 f_0^2 M_E(t)^2}{4\pi^2 \left(2\mu_0 P_{SW}(t) + B_{IMF}^2\right)} \right]^{1/6} \quad (2)$$

where μ_0 is vacuum permeability, f_0 is a field shape parameter for the magnetosphere (1.16 for present day Earth, Voigt (1995), held constant here), and B_{IMF} is the interplanetary field (which is neglected in our calculations since it is small, ≪10 nT). $M_E(t)$ is the (paleo)magnetic dipole moment as a function of time. $P_{SW}(t)$ is the solar wind ram pressure, which is dependent on the mass loss rate of the sun and velocity of solar wind as a function of time. Extrapolating present day P_{SW} (~1.915 nPa; Shue et al., 1997) back through time can be done with power-law model $(t/t_0)^{-2.33}$, where t_0 is the age of Earth (here, 4.54 Gyr), based on solar analogs (e.g., Wood et al., 2005), at least until the young Hadean sun.

Using MCADAM the magnetic standoff distance from 50 ka to 3.7–4.2 Ga can be estimated (Figure 4, Figures S4 and S5 in Supporting Information S1). The magnetopause responds rapidly to changes in either solar wind activity or the geomagnetic field and will vary by ~1 to 2 R_E during typical space weather (Voigt, 1995). Coronal mass ejections and solar flares can suppress the standoff distance by half (e.g., the Halloween 2003 event was observed to reduce the magnetopause to ~5 R_E; Rosenqvist et al., 2005). While short term reductions (≪millions of years) in magnetic shielding are unlikely to impact the biosphere significantly, protracted intervals of reduced shielding may have affected evolutionary processes (e.g., Meert et al., 2016; van der Boon et al., 2022). Our analysis suggests that for the Precambrian the combination of the generally weaker dipole field and the increased solar wind associated with a younger, more active sun resulted in a long-term average standoff of ~6 R_E, which is about 60% the present-day distance and consistent with early Archean estimates (Tarduno et al., 2010). Individual time-averaged estimates (on million-year or shorter timescales) suggest there were intervals with even further reduced standoff distances (e.g., the Ediacaran or Devonian; Meert et al., 2016; van der Boon et al., 2022). These values represent a baseline standoff distance, which could be further reduced due to internal changes in the field (e.g., reduction or loss of dipolarity) or increases in solar wind activity (e.g., coronal mass ejections, solar flares). This implies that during the Precambrian, atmospheric shielding by the magnetic field was potentially tenuous despite the robust, albeit weaker than present day, dipole field.

6. Conclusions

Using an updated PINT database, we have developed a new continuous dipole field modeling approach (MCADAM). Based on three approaches of selection data using Q_{PI} criteria, our MCADAM models can robustly recover the average dipole field strength and captures key features previously identified in the Quaternary, the Mesozoic, and the Precambrian.

Paleomagnetic standoff distance is estimated using our preferred model MCADAM.1b and suggests that following the earliest Archean, the Precambrian standoff distance was ~6 R_E. At the end of the Precambrian, the paleomagnetosphere experienced a protracted (~20 to 100 Myr) minima during the Ediacaran, that was followed by a highly variable, generally (but not monotonically) increasing standoff distance in the Phanerozoic.

The MCADAM models produce a continuous description of the time-averaged paleomagnetic field strength, accompanied by plausible uncertainty bounds defined by the underlying data, spanning an interval starting 50 ka and extending into the earliest Archean. We envision that the MCADAM approach will help bridge the gap between discrete paleomagnetic observations and both geodynamical and paleomagnetospheric investigations that require predictive time series grounded in empirical data sets.

Data Availability Statement

PINT v8.1.1 is available at http://www.pintdb.org/. MCADAM.1a-c model outputs are available in the EarthRef Data Archive at http://www.earthref.org/ERDA/2537/.

Acknowledgments
R.K.B. acknowledges support for The Leverhulme Trust Early Career Fellowship (ECF-2020-617). G.A.P. is funded by a Natural Environment Research Council Independent Research Fellowship (NE/P017266/1). A.J.B acknowledges a Research Leadership Award (RLA-2016-080) provided by The Leverhulme Trust. The authors thank D. Thallner for assistance in merging site records from Eastern Europe. The authors thank Lisa Tauxe and an anonymous reviewer for helpful comments.

References

Biggin, A. J., Bono, R. K., Meduri, D. G., Sprain, C. J., Davies, C. J., Holme, R., & Doubrovine, P. V. (2020). Quantitative estimates of average geomagnetic axial dipole dominance in deep geological time. *Nature Communications*, *11*(1), 6100. https://doi.org/10.1038/s41467-020-19794-7

Biggin, A. J., & Paterson, G. A. (2014). A new set of qualitative reliability criteria to aid inferences on palaeomagnetic dipole moment variations through geological time. *Frontiers of Earth Science*, *2*. https://doi.org/10.3389/feart.2014.00024

Biggin, A. J., Piispa, E. J., Pesonen, L. J., Holme, R., Paterson, G. A., Veikkolainen, T., & Tauxe, L. (2015). Palaeomagnetic field intensity variations suggest Mesoproterozoic inner-core nucleation. *Nature*, *526*(7572), 245–248. https://doi.org/10.1038/nature15523

Biggin, A. J., Strik, G. H. M. A., & Langereis, C. G. (2009). The intensity of the geomagnetic field in the Late-Archaean: New measurements and an analysis of the updated IAGA palaeointensity database. *Earth Planets and Space*, *61*(1), 9–22. https://doi.org/10.1186/BF03352881

Bono, R. K., Paterson, G. A., van der Boon, A., Engbers, Y. A., Michael Grappone, J., Handford, B., et al. (2022). The PINT database: A definitive compilation of absolute palaeomagnetic intensity determinations since 4 billion years ago. *Geophysical Journal International*, *229*(1), 522–545. https://doi.org/10.1093/gji/ggab490

Bono, R. K., Tarduno, J. A., Nimmo, F., & Cottrell, R. D. (2019). Young inner core inferred from Ediacaran ultra-low geomagnetic field intensity. *Nature Geoscience*, *12*(2), 143–147. https://doi.org/10.1038/s41561-018-0288-0

Cleveland, W. S. (1979). Robust locally weighted regression and smoothing scatterplots. *Journal of the American Statistical Association*, *74*(368), 829–836. https://doi.org/10.2307/2286407

Cottrell, R. D., Tarduno, J. A., & Roberts, J. (2008). The Kiaman Reversed Polarity Superchron at Kiama: Toward a field strength estimate based on single silicate crystals. *Physics of the Earth and Planetary Interiors*, *169*(1–4), 49–58. https://doi.org/10.1016/j.pepi.2008.07.041

Di Chiara, A., Tauxe, L., Staudigel, H., Florindo, F., Protti, M., Yu, Y., et al. (2021). Earth's magnetic field strength and the cretaceous normal superchron: New data from Costa Rica. *Geochemistry, Geophysics, Geosystems*, *22*(4), e2020GC009605. https://doi.org/10.1029/2020GC009605

Driscoll, P. E. (2016). Simulating 2 Ga of geodynamo history. *Geophysical Research Letters*, *43*(11), 2016GL068858. https://doi.org/10.1002/2016GL068858

Efron, B., & Tibshirani, R. (1993). *An introduction to the bootstrap*. Chapman & Hall.

Glassmeier, K.-H., & Vogt, J. (2010). Magnetic polarity transitions and biospheric effects. *Space Science Reviews*, *155*(1), 387–410. https://doi.org/10.1007/s11214-010-9659-6

Hawkins, L. M. A., Anwar, T., Shcherbakova, V. V., Biggin, A. J., Kravchinsky, V. A., Shatsillo, A. V., & Pavlov, V. E. (2019). An exceptionally weak Devonian geomagnetic field recorded by the Viluy Traps, Siberia. *Earth and Planetary Science Letters*, *506*, 134–145. https://doi.org/10.1016/j.epsl.2018.10.035

Hawkins, L. M. A., Grappone, J. M., Sprain, C. J., Saengduean, P., Sage, E. J., Thomas-Cunningham, S., et al. (2021). Intensity of the Earth's magnetic field: Evidence for a Mid-Paleozoic dipole low. *Proceedings of the National Academy of Sciences*, *118*(34), e2017342118. https://doi.org/10.1073/pnas.2017342118

Holtzman, W. H. (1950). The unbiased estimate of the population variance and standard deviation. *American Journal of Psychology*, *63*(4), 615–617. https://doi.org/10.2307/1418879

Ingham, E., Heslop, D., Roberts, A. P., Hawkins, R., & Sambridge, M. (2014). Is there a link between geomagnetic reversal frequency and paleointensity? A Bayesian approach. *Journal of Geophysical Research: Solid Earth*, *119*(7), 5290–5304. https://doi.org/10.1002/2014JB010947

Kulakov, E., Sprain, C., Doubrovine, P., Smirnov, A., Paterson, G., Hawkins, L., et al. (2019). Analysis of an updated paleointensity database (Q_{PI}-PINT) for 65-200 Ma: Implications for the long-term history of dipole moment through the Mesozoic. *Journal of Geophysical Research: Solid Earth*, *124*(10), 2018JB017287. https://doi.org/10.1029/2018JB017287

Lloyd, S. J., Biggin, A. J., Halls, H., & Hill, M. J. (2021). First palaeointensity data from the cryogenian and their potential implications for inner core nucleation age. *Geophysical Journal International*, *226*(1), 66–77. https://doi.org/10.1093/gji/ggab090

Meert, J. G., Levashova, N. M., Bazhenov, M. L., & Landing, E. (2016). Rapid changes of magnetic field polarity in the late Ediacaran: Linking the Cambrian evolutionary radiation and increased UV-B radiation. *Gondwana Research*, *34*, 149–157. https://doi.org/10.1016/j.gr.2016.01.001

Merrill, R. T., McElhinny, M. W., & McFadden, P. L. (1996). *The magnetic field of the Earth: Paleomagnetism, the core, and the deep mantle* (Vol. 63). Academic Press.

Nimmo, F. (2015). 9.08 – Thermal and compositional evolution of the core. In G. Schubert (Ed.), *Treatise on geophysics* (2nd ed., pp. 201–219). Elsevier.

Opdyke, N. D., & Channell, J. E. (1996). 12 – Triassic and paleozoic magnetic stratigraphy. In N. D. Opdyke & J. E. Channell (Eds.), *Magnetic stratigraphy* (Vol. 64, pp. 205–232). Academic Press. https://doi.org/10.1016/S0074-6142(06)80014-8

Panovska, S., Constable, C. G., & Korte, M. (2018). Extending global continuous geomagnetic field reconstructions on timescales beyond human civilization. *Geochemistry, Geophysics, Geosystems*, *19*(12), 4757–4772. https://doi.org/10.1029/2018GC007966

Rodríguez-Mozos, J. M., & Moya, A. (2017). Statistical-likelihood Exo-Planetary Habitability Index (SEPHI). *Monthly Notices of the Royal Astronomical Society*, *471*(4), 4628–4636. https://doi.org/10.1093/mnras/stx1910

Rosenqvist, L., Opgenoorth, H., Buchert, S., McCrea, I., Amm, O., & Lathuillere, C. (2005). Extreme solar-terrestrial events of October 2003: High-latitude and cluster observations of the large geomagnetic disturbances on 30 October. *Journal of Geophysical Research*, *110*(A9), A09S23. https://doi.org/10.1029/2004JA010927

Salminen, J., Donadini, F., Pesonen, L. J., Masaitis, V. L., & Naumov, M. V. (2006). Paleomagnetism and petrophysics of the Jänisjärvi impact structure, Russian Karelia. *Meteoritics & Planetary Sciences*, *41*(12), 1853–1870. https://doi.org/10.1111/j.1945-5100.2006.tb00456.x

Savitzky, A., & Golay, M. J. E. (1964). Smoothing and differentiation of data by simplified least squares procedures. *Analytical Chemistry*, *36*(8), 1627–1639. https://doi.org/10.1021/ac60214a047

Selkin, P. A., & Tauxe, L. (2000). Long-term variations in palaeointensity. *Philosophical Transactions of the Royal Society of London, Series A: Mathematical, Physical and Engineering Sciences*, *358*(1768), 1065–1088. https://doi.org/10.1098/rsta.2000.0574

Shue, J.-H., Chao, J. K., Fu, H. C., Russell, C. T., Song, P., Khurana, K. K., & Singer, H. J. (1997). A new functional form to study the solar wind control of the magnetopause size and shape. *Journal of Geophysical Research*, *102*(A5), 9497–9511. https://doi.org/10.1029/97JA00196

Siscoe, G. L., & Chen, C.-K. (1975). The paleomagnetosphere. *Journal of Geophysical Research*, *80*(34), 4675–4680. https://doi.org/10.1029/JA080i034p04675

Siscoe, G. L., & Sibeck, D. G. (1980). Effects of nondipole components on auroral zone configurations during weak dipole field epochs. *Journal of Geophysical Research*, *85*(B7), 3549–3556. https://doi.org/10.1029/JB085iB07p03549

Smirnov, A. V., Tarduno, J. A., Kulakov, E. V., McEnroe, S. A., & Bono, R. K. (2016). Palaeointensity, core thermal conductivity and the unknown age of the inner core. *Geophysical Journal International*, *205*(2), 1190–1195. https://doi.org/10.1093/gji/ggw080

Smith, P. J. (1967). The intensity of the tertiary geomagnetic field. *Geophysical Journal International*, *12*(3), 239–258. https://doi.org/10.1111/j.1365-246X.1967.tb03120.x

Tarduno, J. A., Blackman, E. G., & Mamajek, E. E. (2014). Detecting the oldest geodynamo and attendant shielding from the solar wind: Implications for habitability. *Physics of the Earth and Planetary Interiors*, *233*, 68–87. https://doi.org/10.1016/j.pepi.2014.05.007

Tarduno, J. A., Cottrell, R. D., Bono, R. K., Oda, H., Davis, W. J., Fayek, M., et al. (2020). Paleomagnetism indicates that primary magnetite in zircon records a strong Hadean geodynamo. *Proceedings of the National Academy of Sciences*, *117*(5), 2309–2318. https://doi.org/10.1073/pnas.1916553117

Tarduno, J. A., Cottrell, R. D., Davis, W. J., Nimmo, F., & Bono, R. K. (2015). A Hadean to Paleoarchean geodynamo recorded by single zircon crystals. *Science*, *349*(6247), 521–524. https://doi.org/10.1126/science.aaa9114

Tarduno, J. A., Cottrell, R. D., Watkeys, M. K., Hofmann, A., Doubrovine, P. V., Mamajek, E. E., et al. (2010). Geodynamo, solar wind, and magnetopause 3.4 to 3.45 billion years ago. *Science*, *327*(5970), 1238–1240. https://doi.org/10.1126/science.1183445

Tauxe, L., & Staudigel, H. (2004). Strength of the geomagnetic field in the cretaceous normal superchron: New data from submarine basaltic glass of the troodos Ophiolite: Cretaceous Normal Superchron. *Geochemistry, Geophysics, Geosystems*, *5*(2), Q02H06. https://doi.org/10.1029/2003GC000635

Thallner, D., Biggin, A. J., & Halls, H. C. (2021). An extended period of extremely weak geomagnetic field suggested by palaeointensities from the Ediacaran Grenville dykes (SE Canada). *Earth and Planetary Science Letters*, *568*, 117025. https://doi.org/10.1016/j.epsl.2021.117025

Thallner, D., Biggin, A. J., McCausland, P. J. A., & Fu, R. R. (2021). New paleointensities from the skinner cove formation, Newfoundland, suggest a changing state of the geomagnetic field at the Ediacaran-Cambrian transition. *Journal of Geophysical Research: Solid Earth*, *126*(9), e2021JB022292. https://doi.org/10.1029/2021JB022292

Thallner, D., Shcherbakova, V. V., Bakhmutov, V. G., Shcherbakov, V. P., Zhidkov, G. V., Poliachenko, I. B., & Biggin, A. J. (2022). New palaeodirections and palaeointensity data from extensive profiles through the Ediacaran section of the Volyn Basalt Province (NW Ukraine). *Geophysical Journal International*, *231*(1), 474–492. https://doi.org/10.1093/gji/ggac186

van der Boon, A., Biggin, A. J., Thallner, D., Hounslow, M. W., Bono, R., Nawrocki, J., et al. (2022). A persistent non-uniformitarian paleomagnetic field in the Devonian? *Earth-Science Reviews*, *231*, 104073. https://doi.org/10.1016/j.earscirev.2022.104073

Voigt, G.-H. (1995). Magnetospheric configuration. In *Handbook of atmospheric electrodynamics* (1st ed., Vol. 2, pp. 333–388). CRC Press. https://doi.org/10.1201/9780203713297-11

Wood, B. E., Müller, H.-R., Zank, G. P., Linsky, J. L., & Redfield, S. (2005). New mass-loss measurements from Astrospheric Lyα absorption. *The Astrophysical Journal Letters*, *628*(2), L143–L146. https://doi.org/10.1086/432716

Zhou, T., Tarduno, J. A., Nimmo, F., Cottrell, R. D., Bono, R. K., Ibanez-Mejia, M., et al. (2022). Early Cambrian renewal of the geodynamo and the origin of inner core structure. *Nature Communications*, *13*(1), 4161. https://doi.org/10.1038/s41467-022-31677-7

Ziegler, L. B., Constable, C. G., Johnson, C. L., & Tauxe, L. (2011). PADM2M: A penalized maximum likelihood model of the 0–2 Ma palaeomagnetic axial dipole moment. *Geophysical Journal International*, *184*(3), 1069–1089. https://doi.org/10.1111/j.1365-246X.2010.04905.x

References From the Supporting Information

Abdulghafur, F., & Bowles, J. A. (2019). Absolute paleointensity study of Miocene Tiva Canyon Tuff, Yucca Mountain, Nevada: Role of fine-particle grain-size variations. *Geochemistry, Geophysics, Geosystems*, *20*(12), 5818–5830. https://doi.org/10.1029/2019GC008728

Asefaw, H., Tauxe, L., Koppers, A. a. P., & Staudigel, H. (2021). Four-dimensional paleomagnetic dataset: Plio-pleistocene paleodirection and paleointensity results from the Erebus volcanic Province, Antarctica. *Journal of Geophysical Research: Solid Earth*, *126*(2), e2020JB020834. https://doi.org/10.1029/2020JB020834

Biasi, J., Kirschvink, J. L., & Fu, R. R. (2021). Characterizing the geomagnetic field at high southern Latitudes: Evidence from the Antarctic Peninsula. *Journal of Geophysical Research: Solid Earth*, *126*(12), e2021JB023273. https://doi.org/10.1029/2021JB023273

Calvo-Rathert, M., Bógalo, M. F., Morales, J., Goguitchaichvili, A., Lebedev, V. A., Vashakidze, G., et al. (2021). An integrated paleomagnetic, multimethod-paleointensity, and radiometric study on Cretaceous and Paleogene lavas from the Lesser Caucasus: Geomagnetic and tectonic implications. *Journal of Geophysical Research: Solid Earth*, *126*(2), e2020JB020019. https://doi.org/10.1029/2020JB020019

Cervantes-Solano, M., Goguitchaichvili, A., Sánchez Bettucci, L., Morales-Contreras, J., Gogorza, C., & Núñez, P. (2020). An integrated paleomagnetic and multispecimen paleointensity study from the late Jurassic Zapicán dike swarm (Uruguay). *Journal of South American Earth Sciences*, *104*, 102815. https://doi.org/10.1016/j.jsames.2020.102815

Chang, B., Kim, W., Doh, S.-J., & Yu, Y. (2013). Paleointensity determination of Late Cretaceous basalts in northwest South Korea: Implications for low and stable paleofield strength in the Late Cretaceous. *Earth Planets and Space*, *65*(12), 1501–1513. https://doi.org/10.5047/eps.2013.09.013

Chauvin, A., Roperch, P., & Levi, S. (2005). Reliability of geomagnetic paleointensity data: The effects of the NRM fraction and concave-up behavior on paleointensity determinations by the Thellier method. *Physics of the Earth and Planetary Interiors*, *150*(4), 265–286. https://doi.org/10.1016/j.pepi.2004.11.008

Døssing, A., Muxworthy, A. R., Supakulopas, R., Riishuus, M. S., & Mac Niocaill, C. (2016). High northern geomagnetic field behavior and new constraints on the Gilsá event: Paleomagnetic and $^{40}Ar/^{39}Ar$ results of ∼0.5–3.1 Ma basalts from Jökuldalur, Iceland. *Earth and Planetary Science Letters*, *456*, 98–111. https://doi.org/10.1016/j.epsl.2016.09.022

Eitel, M., Gilder, S. A., Spray, J., Thompson, L., & Pohl, J. (2016). A paleomagnetic and rock magnetic study of the Manicouagan impact structure: Implications for crater formation and geodynamo effects. *Journal of Geophysical Research: Solid Earth*, *121*(2), 436–454. https://doi.org/10.1002/2015JB012577

Eliseev, A., Shcherbakova, V., Metelkin, D., Mikhaltsov, N., Zhidkov, G., Abashev, V., & Rogov, A. (2021). Low geomagnetic field paleointensity on the Permian–Triassic boundary from study of the Kuznetsk Basin Traps (Southern Siberia). *Russian Geology and Geophysics*, *63*(2), 193–207. https://doi.org/10.2113/RGG20204330

Engbers, Y. A., Grappone, J. M., Mark, D. F., & Biggin, A. J. (2022). Low paleointensities and Ar/Ar ages from Saint Helena provide evidence for recurring magnetic field weaknesses in the South Atlantic. *Journal of Geophysical Research: Solid Earth*, *127*(3), e2021JB023358. https://doi.org/10.1029/2021JB023358

Goguitchaichvili, A., Alva-Valdivia, L. M., Urrutia-Fucugauchi, J., Morales, J., & Ferrari, L. (2000). Absolute palaeointensity results from the Trans-Mexican Volcanic Belt: Implications for the late Miocene geomagnetic field strength. *Geophysical Journal International*, *143*(3), 977–984. https://doi.org/10.1046/j.1365-246X.2000.01301.x

Kapawar, M. R., & Mamilla, V. (2021). Paleointensity of the Earth's magnetic field at ∼117 Ma determined from the Rajmahal and Sylhet Trap Basalts, India. *Journal of Earth System Science*, *130*(3), 154. https://doi.org/10.1007/s12040-021-01652-9

Lloyd, S. J., Biggin, A. J., & Li, Z.-X. (2021). New paleointensity data suggest possible phanerozoic-type paleomagnetic variations in the Precambrian. *Geochemistry, Geophysics, Geosystems*, *22*(10), e2021GC009990. https://doi.org/10.1029/2021GC009990

Lloyd, S. J., Biggin, A. J., Paterson, G. A., & McCausland, P. J. A. (2022). Extremely weak early Cambrian dipole moment similar to Ediacaran: Evidence for long-term trends in geomagnetic field behaviour? *Earth and Planetary Science Letters*, *595*, 117757. https://doi.org/10.1016/j.epsl.2022.117757

Mahgoub, A. N., García-Amador, B. I., & Alva-Valdivia, L. M. (2021). Comprehensive palaeomagnetic study of San Borja and Jaraguay monogenetic volcanic fields, Baja California (28–30°N): Considerations on latitudinal corrections. *Geophysical Journal International*, *225*(3), 1897–1919. https://doi.org/10.1093/gji/ggab064

Meng, J., Lhuillier, F., Wang, C., Liu, H., Eid, B., & Li, Y. (2020). Paleomagnetism of Paleocene-Maastrichtian (60–70 Ma) lava flows from Tian Shan (Central Asia): Directional analysis and paleointensities. *Journal of Geophysical Research: Solid Earth*, *125*(9), e2019JB018631. https://doi.org/10.1029/2019JB018631

Miki, M., Seki, H., Yamamoto, Y., Gouzu, C., Hyodo, H., Uno, K., & Otofuji, Y.-I. (2020). Paleomagnetism, paleointensity and geochronology of a Proterozoic dolerite dyke from southern West Greenland. *Journal of Geodynamics*, *139*, 101752. https://doi.org/10.1016/j.jog.2020.101752

Radhakrishna, T., Asanulla, M. R., Venkateshwarlu, M., & Soumya, G. S. (2020). Low geomagnetic field strength during End-Cretaceous Deccan volcanism and whole mantle convection. *Scientific Reports*, *10*(1), 10743. https://doi.org/10.1038/s41598-020-67245-6

Sánchez-Moreno, E. M., Calvo-Rathert, M., Goguitchaichvili, A., Tauxe, L., Vashakidze, G. T., & Lebedev, V. A. (2020). Weak palaeointensity results over a Pliocene volcanic sequence from Lesser Caucasus (Georgia): Transitional record or time averaged field? *Geophysical Journal International*, *220*(3), 1604–1618. https://doi.org/10.1093/gji/ggz533

Sánchez-Moreno, E. M., Calvo-Rathert, M., Goguitchaichvili, A., Vashakidze, G. T., Camps, P., Morales-Contreras, J., et al. (2021). Paleointensity results from Pliocene lavas of the Lesser Caucasus obtained using the multispecimen parallel differential pTRM method: A comparison with Thellier-Thellier and IZZI data. *Journal of Geophysical Research: Solid Earth*, *126*(4), e2020JB019682. https://doi.org/10.1029/2020JB019682

Schnepp, E., Arneitz, P., Ganerød, M., Scholger, R., Fritz, I., Egli, R., & Leonhardt, R. (2021). Intermediate field directions recorded in Pliocene basalts in Styria (Austria): Evidence for cryptochron C2r.2r-1. *Earth Planets and Space*, *73*(1), 182. https://doi.org/10.1186/s40623-021-01518-w

Shcherbakova, V. V., Bakhmutov, V. G., Thallner, D., Shcherbakov, V. P., Zhidkov, G. V., & Biggin, A. J. (2020). Ultra-low palaeointensities from East European Craton, Ukraine support a globally anomalous palaeomagnetic field in the Ediacaran. *Geophysical Journal International*, *220*(3), 1928–1946. https://doi.org/10.1093/gji/ggz566

Tauxe, L., Asefaw, H., Behar, N., Koppers, A. A. P., & Shaar, R. (2022). Paleointensity estimates from the Pleistocene of northern Israel: Implications for hemispheric asymmetry in the time-averaged field. *Geochemistry, Geophysics, Geosystems*, *23*(9), e2022GC010473. https://doi.org/10.1029/2022GC010473

Yoshimura, Y., Yamazaki, T., Yamamoto, Y., Ahn, H.-S., Kidane, T., & Otofuji, Y.-i. (2020). Geomagnetic paleointensity around 30 Ma estimated from Afro-Arabian Large Igneous Province. *Geochemistry, Geophysics, Geosystems*, *21*(12), e2020GC009341. https://doi.org/10.1029/2020GC009341

Zhang, Y., Swanson-Hysell, N. L., Avery, M. S., & Fu, R. R. (2022). High geomagnetic field intensity recorded by anorthosite xenoliths requires a strongly powered late Mesoproterozoic geodynamo. *Proceedings of the National Academy of Sciences of the United States of America*, *119*(29), e2202875119. https://doi.org/10.1073/pnas.2202875119